Bond-switching mechanism for the zircon-scheelite phase transition

M. B. Smirnov,[1] A. P. Mirgorodsky,[2] V. Yu. Kazimirov,[3,4] and R. Guinebretière[2]
[1]*Fock Institute of Physics, Saint-Petersburg State University, Petrodvoretz, 194508 St.-Petersburg, Russia*
[2]*Laboratoire de Science des Procédés Céramiques et de Traitements de Surface, ENSCI, UMR 6638, 47-73 Avenue Albert Thomas, 87065 Limoges Cedex, France*
[3]*Joint Institute for Nuclear Research, 141980 Dubna, Russia*
[4]*Department of Physics, University of Virginia, Charlottesville, Virginia 22904-4714, USA*
(Received 28 July 2007; revised manuscript received 25 July 2008; published 22 September 2008)

The stress-induced zircon-scheelite phase transition is theoretically studied by means of *ab initio* and shell-model calculations. It is shown that this phase transition may originate from shear elastic strains which bring together the structures of both phases and draw them unstable against the SiO_4-tetrahedron rotations necessary for direct and inverse conversions. As a result, a structural catastrophe occurs within the ZrO_8 polyhedrons: part of the Zr-O bonds disrupts and new ones form. Such a "bond switching" is crucial for the first-order reconstructive character of the transition which, according to this study, would proceed via the $D_{4h}^{19}-D_{2h}^{24}-C_{2h}^{6}-C_{4h}^{6}$ symmetry group succession.

DOI: 10.1103/PhysRevB.78.094109 PACS number(s): 68.18.Jk, 61.50.Ah

I. INTRODUCTION

A wide range of the first-order structural phase transitions (SPTs) in solids can be characterized as reconstructive ones. This term usually implies that the arrangement of interatomic bonds necessarily changes (is *reconstructed*) during the transition, thus varying coordination polyhedrons around the atoms. Theoretical treatment of reconstructive SPTs is a much more difficult problem than that of second-order "soft" SPTs which involve only low-scale structural distortions and maintain the group-subgroup relation between parent and daughter phases. No valence bonds are broken, and coordination polyhedrons do not change during these SPTs.

Recently, extension of the symmetry group-subgroup relation to reconstructive SPT was proposed, allowing recovery of the order-parameter concept through the idea of a low-symmetry intermediate transition state.[1] Microscopic modeling of reconstructive transformations is based on the consideration of the collective displacement of atoms preserving long-range translational symmetry. This implies that thermodynamic potentials must be theoretically calculated for different structural configurations along the transformation path (TP). The quest for a probability hierarchy among possible TPs should include calculation of the free-energy variation as well as quantitative estimates of kinetic parameters, such as activation energies and volume drops.[2,3]

At present, our understanding of the driving forces involved in reconstructive transformation remains limited even for relatively simple binary AX compounds. Extensive studies of pressure-induced phase transformations from the fourfold coordinated (zinc blend or wurtzite) to the sixfold coordinated (NaCl-type) structures, and from the latter to the eightfold coordinated (CsCl-type) structures, have shown that the set of alternative paths might be plenty. Therefore, the TP sampling procedure inevitably involves a huge amount of the energy calculations.

For many pressure-induced reconstructive SPT occurring at room temperature, theoretical estimation of critical pressure obtained from enthalpy equality condition can correspond reasonably to experimental data only if the activation energy (the height of energy barrier separated the two energy minima) is sufficiently low. Generally speaking, it is not the case for the SPTs with relatively high-energy barriers. As a rule, such SPTs manifest sluggish character: the pressure interval between the onset and the completion of a transformation is quite large, and the high-pressure phase is quenched upon pressure release. The wurtzite to rocksalt transformation in AlN,[3] the amorphization in SiO_2,[4] and the zircon-scheelite transformation in ABO_4 compounds[5–7] are examples. In this case, when thermodynamically metastable parent phase may persist throughout a wide pressure interval above P_c, knowledge of the lattice-dynamical properties of this phase can be very useful in order to correctly predict its behavior.[4,8,9] Indeed, analysis of the phonon spectrum and elastic modulus makes it possible to reveal incipient pressure-induced structural instabilities, which can eventually induce a continuous evolution from one phase to the other at a pressure higher than P_c. In principle, then, the optimal path through a transition enthalpy barrier can be found in this way. Moreover, the role of vibrational states in phase-transition mechanism can be clarified.

However, not infrequently analysis of the violation of Born's stability criteria in an isotropically compressed lattice is insufficient to understand behavior of this "highly persistent" metastable structure.[4] Rather, nonhydrostatic stresses were found to significantly influence the onset of transformation. This implies that anisotropic strains might be induced in abundance in a compressed sample (especially a powdered sample), and that the daughter structure might nucleate spontaneously around such stress fluctuation domains with no obvious deformation of the parent phase.

The $ZrSiO_4$ zircon lattice (z phase) is known to undergo a pressure-induced SPT to a scheelitelike lattice (s phase) called reidite.[10] A series of other ABO_4 compounds including vanadates[5] and chromates[6] manifest similar behavior, allowing one to suppose that a pressure-induced $z-s$ transformation is a property common to this family of structures. The standard crystallographic unit cells of the z phase (D_{4h}^{19}; a_t

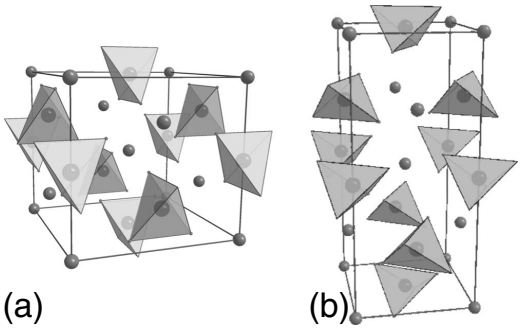

FIG. 1. Crystal structures of (a) zircon and (b) reidite. SiO_4 units are shown as tetrahedrons, and Zr atoms are shown as balls.

$=b_t=6.645$ Å, $c_t=6.015$ Å; $Z=4$) and *s* phase (C_{4h}^6; $a_t=b_t=4.734$ Å, $c_t=10.51$ Å; $Z=4$) of $ZrSiO_4$ are shown in Fig. 1. It is seen that neither zirconium atoms nor the silicon atoms change their positions in the cell during the transition. Meanwhile, the oxygen atom arrangement retains the shapes of the SiO_4 and ZrO_8 polyhedrons. Such structural similarity and a clear group-subgroup symmetry correlation between the lattices suggest that the $z-s$ transformation could be largely explained as a second-order SPT with the order parameter belonging to the A_{2g} irreducible representation of the D_{4h} group, which should involve rotations of the SiO_4 tetrahedrons. However a more detailed analysis of the experimental data[7,10–17] concerning the structural, thermodynamic, and mechanic aspects of this transformation supports its first-order character.

The $z-s$ SPT was observed for the first time in high-temperature experiments at pressures around 10 GPa.[10] The relevant Clayperon slope dP_c/dT was found to be positive, giving P_c of about 6 GPa at $T=0$ K.[16] At the same time, room-temperature/high-pressure experiments showed that the *z* phase persists at pressures higher than 20 GPa.[7,17,18] A Raman spectroscopy study[7] revealed new spectral features which could indicate the onset of a pressure-induced structural phase transition at 13 GPa. However, considerable overdriving in pressure (up to 23 GPa) is needed to complete the transformation. It was also found that the high-pressure born *s*-phase persists upon pressure release but returns quickly to zircon when heated to 1500 K. Experimental data collected so far clearly show that the $z-s$ and $s-z$ transformations are kinetically hindered. This means that the transformation is governed by the thermodynamic equilibrium condition only at sufficiently high temperatures where the parent and product phases are close to equilibrium and the energetic barriers associated with these transformations can be easily overcome due to thermal fluctuations. Both $z-s$ and $s-z$ inversions can be identified thus as first-order SPTs with rather high activation entropy and high persistence of the metastable phases. Theoretical treatment of the inversions, then, should involve joint analysis of enthalpy barrier and Born's stability criteria and should pay particular attention to the role of nonhydrostatic stresses.

Some ABO_4 compounds having a zircon or scheelite structure are important materials in the engineering of solid-state scintillator detectors, optoelectronic devices, and solid-state lasers. As for the "father" structure $ZrSiO_4$, it is of great geophysical interest as an important host mineral for heat producing radioactive elements in the Earth's crust.[16] It can be added that zircon is of the great utility in the ceramics industry, thanks to a series of remarkable thermal and mechanical properties: low thermal conductivity, high melting point, low thermal expansion, and good thermal shock resistance. The compressibility and thermal expansion of zircon are the lowest among the oxygen-based compounds. In particular, it was noted that the *s*-phase $ZrSiO_4$ is one of the most incompressible compounds containing SiO_4 tetrahedral.[15]

Understanding the nature of the $z-s$ SPT is important both theoretically and for industrial application. Indeed, this crystal structure is more complex than the two-atomic ones widely studied as model systems undergoing reconstructive SPT. It can be thought that revealing the mechanism for the $z-s$ transformation would contribute significantly to theory of the first-order reconstructive SPT at the level of both fundamental principles and modeling strategy. Our investigation into the nature of the $z-s$ phase transition is not the first. Rather, we would like to argue in this paper that despite a series of previous theoretical studies,[18–21] the question on microscopic mechanism of this SPT is still very far from clarity.

II. COMPUTATIONAL METHODS

The results of previous theoretical studies using density-functional theory (DFT) (Refs. 18 and 19) and the empirical shell model[20,21] were in line with experiment insofar as they satisfactorily reproduced the equilibrium structures and dynamical properties of both polymorphs. In this study, we used similar computational techniques. The program CASTEP (Ref. 22) was used for the DFT calculations. We employed the revised Perdew-Burke-Ernzerhof exchange-correlation functional[23] for generalized gradient approximation. Monkhorst-Pack grids contained up to $6\times6\times7$ *k* points to allow greater accuracy. Core electrons were simulated by norm-conserving pseudopotentials.[24] The shell-model (SM) potential developed by Mittal *et al.*[21] was used for the lattice dynamics simulations.

III. RESULTS AND DISCUSSION

A. Stability under pressure

First of all, we studied the role of volume variation which is usually an important (if not crucial) factor for a pressure-induced SPTs. $E(V)$ dependencies for both structures as calculated by the DFT and SM methods are shown in Figs. 2(a) and 2(b), respectively (E is the potential energy and V is the specific volume). These calculations included the geometry optimization over all structural parameters other than unit-cell volume. Such calculations are equivalent to simulation of structural evolution under an external pressure (corresponding pressure values can be determined as the derivative $P=-dE/dV$).

Absolute energy values given by the SM cannot be compared with quantum-mechanical energies derived from *ab initio* calculations. However, the SM parameters were ad-

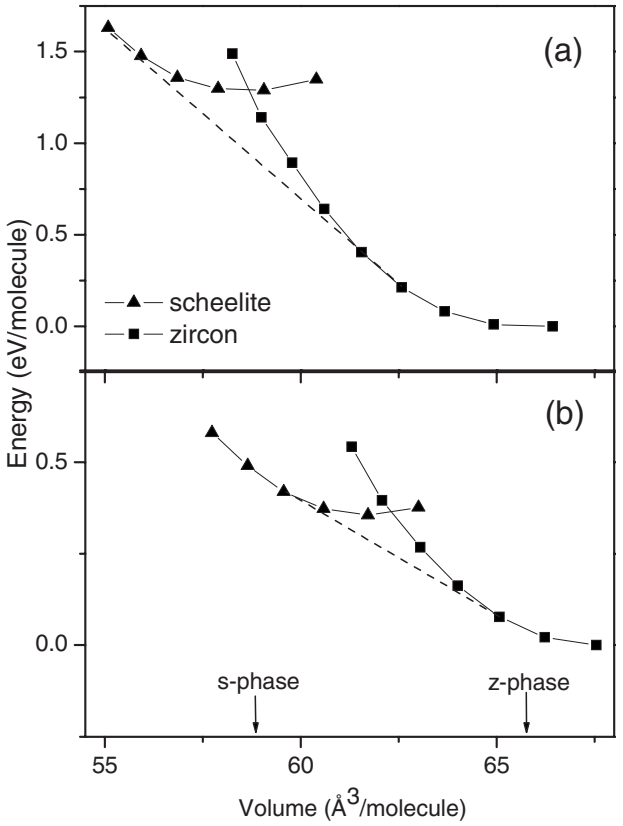

FIG. 2. Energy versus volume dependencies for the z-phase (squares) and s-phase (triangles) structures calculated by (a) DFT and (b) SM methods. Common tangents are shown in the figures as dashed lines. Points are plotted in intervals of 5 GPa at pressures ranging from 0 GPa for the z phase and from −5 GPa for the s phase. Vertical arrows indicate the experimental values of specific volumes of the two polymorphs at zero pressure.

justed in such a way as to provide reasonable values of energy variations related to structural variations. In order to compare results obtained by the two methods, only relative energy values will be discussed. The zero-energy level is assigned to the energy of the z phase in its energy minimum configuration. Thus, the energy values discussed in the paper correspond to the energy of elastic strains relative to the absolute energy minimum. Hereinafter this strain energy is referred to as deformation energy.

It is seen in Fig. 2 that the two $E_z(V)$ and $E_s(V)$ curves in Fig. 2 intersect but never merge. This fact clearly shows that the two lattices can never simultaneously share three coinciding thermodynamic parameters: potential energy, volume, and pressure. This fact points to the first-order character of the SPT.

Since SPT under consideration is induced by increasing external pressure at room temperature, it can be suggested that the relevant theoretical modeling can be simplified by assuming that $T=0$ K. In such a case, the free energy can be replaced by enthalpy $H=E+PV$. Theoretical estimate of the critical pressure P_c was obtained from the condition $H_z(P)=H_s(P)$. Graphically, this condition is equivalent to the common tangent construction represented in Fig. 2 by dashed lines According to the DFT (SM) results shown in Fig. 2(a) [Fig. 2(b)], the thermodynamic equilibrium condition would occur at P_c equal to 15 (10) GPa with the z-phase volume exceeding that of the s phase by 10% (8.5%), respectively. However, the enthalpy equality is a necessary but not sufficient condition for SPT. If at $P=P_c$ both structures are mechanically stable, the probability of a transformation is determined by the height of the energy barrier and by the ability of the system to overcome this barrier.

We studied the effect of volume variation on mechanic stability of both phases. For this purpose, phonon frequencies and elastic constants have been calculated in a wide pressure interval. No marked phonon softening was found: frequencies of all zone-center phonons remain higher than 100 cm^{-1} at pressures up to 100 GPa. The only exception is the B_{2u} mode of the z phase. Its frequency goes to zero at 24 (50) GPa according to DFT (SM) calculations. However, this does not lead to drastic structural reconstruction but to a soft second-order SPT involving small-scale antiphase rotations of neighboring SiO_4 tetrahedra around the tetragonal axis and a symmetry change from D_{4h}^{19} to D_{2d}^{12}. Since this SPT is predicted to occur at rather high pressure and results in minor alterations of structural and lattice-dynamical properties of the z phase, we will neglect it in the forthcoming analysis.

The stability of a lattice with respect to homogeneous deformations was tested by analysis of the eigenvalues of the elastic constant matrix (hereinafter in this paper these quantities are referred to as the elastic moduli). It was found that all the elastic moduli increase with pressure. The only exception is the C_{66} modulus in the z phase, which decreases and then vanishes at $P\sim 70$ GPa. Therefore, it can be concluded that in a wide pressure interval extending to pressures much greater than P_c both structures are mechanically stable. Neither the experimental data nor the theoretical calculation reveals any indication of the disappearance of the $z-s$ energy barrier under hydrostatic compression or of any predisposition to instability in response to pressure values as much as two to three times greater than P_c values observed experimentally or predicted by thermodynamic equilibrium condition. This means that the potential-energy surface of the $ZrSiO_4$ lattice in this pressure interval is characterized by a coexistence of two steep minima corresponding to the two phases under consideration.

B. Potential surface analysis and transformation path sampling

Theoretical treatment of the first-order SPT requires identification of a TP which interconnects the two minima over the lowest energy barrier possible. To find such a TP, the area of a potential surface between the two minima must be quantitatively analyzed. First, a coordinate space must be chosen such that the potential surface can be represented in a simple but physically meaningful manner. In our case, the $z-s$ phase transition is accompanied by a dramatic variation of the lattice cell parameters but not of relative atomic positions. Therefore, it is our belief that the potential surface can be considered in the coordinate space of the unit-cell parameters; at any point along the TP, corresponding atomic positions can be determined by energy minimization. However,

even this relatively simple approach was found to be computationally expensive for *ab initio* calculations, and our analysis was necessarily limited to SM calculations.

According to the results of Sec. III A, the hydrostatic pressure cannot play an important role in driving the transformation. Therefore, a potential-surface analysis assuming $P=0$ can provide a simple but quite reasonable first approximation (pressure effect will be considered afterwards). In fact, as it is shown below, only two TPs were found warranting a detailed quantitative analysis.

1. Transformation path A (TPA)

By this term we denote a macroscopic homogeneous deformation which directly transforms the tetragonal unit cell of the z phase with $a_t=b_t=6.623$ Å and $c_t=6.164$ Å [Fig. 1(a)] into the tetragonal unit cell of the s phase with $a_t=b_t=4.775$ Å and $c_t=10.830$ Å [Fig. 1(b)], and vice versa (hereinafter we cite the values calculated by SM model). The ratio $\chi=c_t/a_t$ was used as a coordinate of transformation for TPA. We have come from the two terminal points, i.e., from the energy minimum configurations of the z phase ($\chi=0.93$) and the s phase ($\chi=2.27$), and passed along the TPA by gradually changing the χ value in the interval $0.93\leq\chi\leq2.27$, every time optimizing the lattice geometry with respect to all the other structural parameters (keeping $P=0$). This procedure is equivalent to a simulation of structural evolution under external anisotropic stresses,

$$\mathbf{S}_1=(S,S,-2S,0,0,0). \tag{1}$$

Hereinafter, presentation of the stress vector implies the use of the six Voigt's indices. Recall that a positive sign of S corresponds to external stress extending the lattice. Consequently, the S values in Eq. (1) are positive for s phase and negative for z phase.

The calculated $E_z(\chi)$ and $E_s(\chi)$ curves are presented in Fig. 3(a). It is seen that they merge together at $\chi\approx1.625$, indicating the identity of the structures of both phases at this point. The frequency of one of the zone-center phonon modes vanishes at approaching this point from both sides [see Fig. 3(b)]. This mode belongs to the A_{2g} representation in the z phase and to the A_g species in the s phase. It involves the in-phase rotations of the SiO_4 tetrahedrons around the c axis. Thus it can be concluded that along TPA at $\chi\approx1.625$ the second-order displacive SPT would occur giving rise to the $D_{4h}-C_{4h}$ symmetry variation.

It should be emphasized that the point of the summit of the energy barrier with $\chi=\sqrt{2}$ does not correspond to any particular anomaly. However, this point is of a special interest for us. Actually, for $\chi=\sqrt{2}$, the structure of the z phase can be considered as a cubic lattice with twice bigger unit cell whose basic vectors relate to those of the tetragonal unit cell as follows:

$$\mathbf{a}=\mathbf{a}_t+\mathbf{b}_t,\quad \mathbf{b}=\mathbf{a}_t-\mathbf{b}_t,\quad \text{and}\quad \mathbf{c}=\mathbf{c}_t. \tag{2}$$

Analysis of this cubic structure showed that it corresponds to the $Fd\bar{3}m$ (O_h^7) space group and can be described as a superposition of two interpenetrating lattices of ZrO_2 and SiO_2 isomorphous to β-cristobalit which are shifted one against another for $(\frac{1}{2}00)$. This cubic structure can be considered as a virtual transition state, i.e., a highest symmetry protostructure which can be smoothly transformed into both polymorphs. Calculated potential energy of this structure (2.9516 eV/molecule) provides us an estimate of activation energy for TPA.

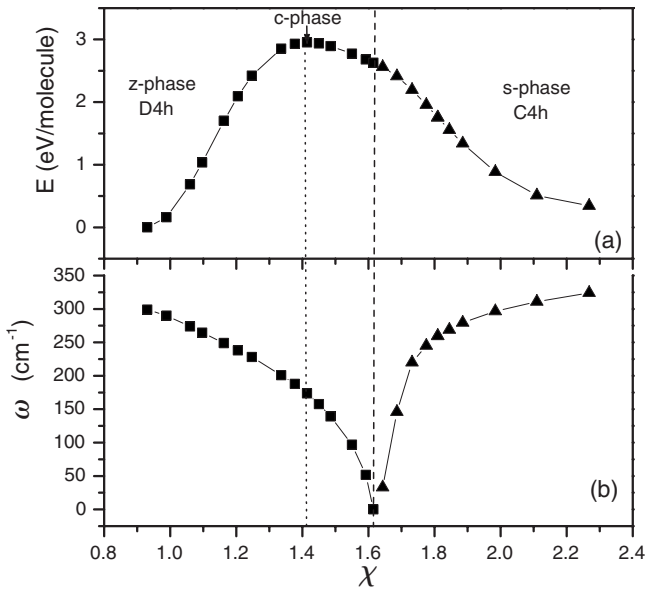

FIG. 3. Plots of (a) potential energy and (b) soft-mode frequency along the TPA as a function of χ. The point of the $D_{4h}^{19}-C_{4h}^6$ phase transition is represented as a vertical dashed line, while the energy maximum is shown as a vertical dotted line.

Hereinafter we shall call the unit cell defined by Eq. (2) as the c cell and use it as a universal extended unit cell for a unified description of all the crystalline structures related to the z- and s-phase lattices along arbitrary TP. According to our calculations, the c-cell parameters of the cubic O_h^7 structure of $ZrSiO_4$ are

$$a=b=c=8.274\ \text{Å}, \tag{3}$$

whereas for the optimized z-phase structure they are

$$a=b=9.366\ \text{Å},\quad c=6.164\ \text{Å}, \tag{4}$$

and for the optimized s-phase structure they are

$$a=b=6.753\ \text{Å},\quad c=10.830\ \text{Å}. \tag{5}$$

Since the three mutually orthogonal fourfold rotation axes of the cubic c cell are equivalent, each of them can theoretically be considered as a germ of the C_4 axis for the z- or s-phase structures. Thus, when using the unified set of the **a**, **b**, and **c** vectors, the tetragonal lattices can be specified by three differently oriented but physically equivalent c cells corresponding to the three possible directions of their C_4 axes. In line with this, the calculated c-cell parameters of the structures in question can be presented as follows:

$$\begin{array}{ccc} z \text{ phase} & c \text{ phase} & s \text{ phase} \\ (6.164,9.366,9.366) & & (10.830,6.753,6.753) \\ (9.366,6.164,9.366) & \Leftrightarrow (8.274,8.274,8.274) \Leftrightarrow & (6.753,10.830,6.753) \\ (9.366,9.366,6.164) & & (6.753,6.753,10.830) \end{array} \quad (6)$$

To unequivocally determine by which unit cell a given structure is specified, we shall use the subindices indicating the orientation of its tetragonal axes (for example, S_a will denote the s lattice in which the tetragonal axes are chosen parallel to **a**). For example, the considered above TPA trajectory has connected the configurations Z_c and S_c and involved the following variation of the c-cell parameters:

$$(9.366,9.366,6.164) \Leftrightarrow (6.753,6.753,10.830). \quad (7)$$

Evidently, the transformations $Z_a \Leftrightarrow S_a$ and $Z_b \Leftrightarrow S_b$ are equivalent to this.

The relations presented in schema (6) mean that, along with the just-mentioned three TPA transformations keeping the orientations of the tetragonal axes, the six other equivalent TPs connecting the configurations with mutually perpendicular tetragonal axes (e.g., $Z_a \Leftrightarrow S_b$, $Z_a \Leftrightarrow S_c$, etc.) must be considered. The seven sets of the c-cell parameters given in schema (6) determine seven points in the configuration space specified by the **a**, **b**, and **c** vectors. The projections of those points on the plane orthogonal to the (111) direction of this space are shown in Fig. 4. They are situated on two circles (different for the z phase and the s phase) surrounding the C point corresponding to the O_h^7 cubic lattice.

The potential curve corresponding to the TPA is a cross section of the potential surface along the line connecting the points $Z_a - C - S_a$ (it is shown in Fig. 4 by the wavy line for better visualization). Figure 4 clearly shows that the lines directly interconnecting the nearest neighbors (e.g., S_a and Z_c) represent the six TP other than TPA. Those TP are physically equivalent and represent an alternative to TPA. We call this alternative as TPB.

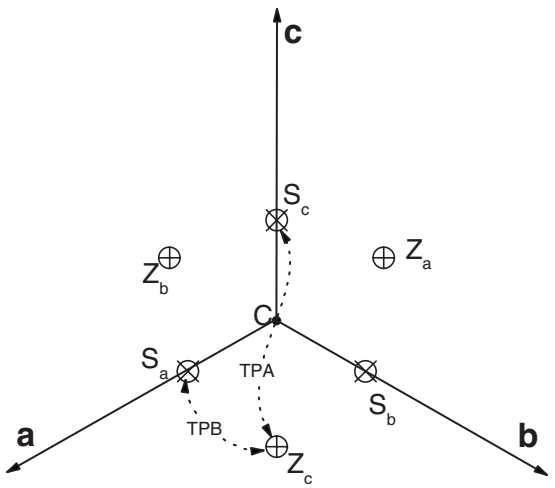

FIG. 4. Positions of various z-phase and s-phase structures in configuration space (abc coordinate system viewed from the [111] direction). Point C corresponds to the prototypical cubic configuration. Trajectories of the TPA and TPB transformations are depicted schematically as dotted curves.

2. Transformation path B (TPB)

In regarding the traces of TPA and TPB in Fig. 4, it is seen that whereas the former inevitably passes through the C point related to the maximum of the potential surface, the latter would go past this point. Moreover, comparing the limiting points of TPB, e.g., those corresponding to the path $Z_a - S_a$,

$$\begin{array}{ccc} Z_c & & S_a \\ (9.366,9.366,6.164) & \Leftrightarrow & (10.830,6.753,6.753) \end{array}, \quad (8)$$

with the analogous points of TBA given by Eq. (7), one can see that TPB would involve lesser uniform strains than TPA. These facts allow us to think that the energy barrier corresponding to the TPB can be lower, and consequently, this path is more thermodynamically preferable. So it is worthy of more detailed consideration.

Transformation path B interconnecting the points Z_c and S_a can be quantitatively characterized by analyzing the potential function $E(a,b,c)$ in the area of the configuration

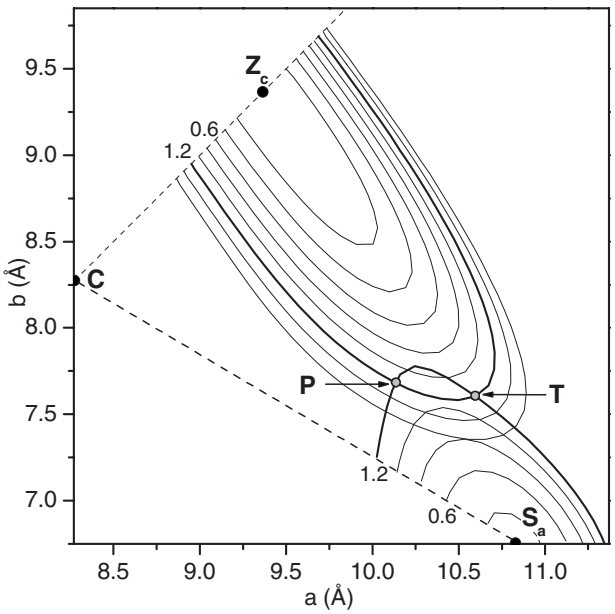

FIG. 5. Cross sections viewed from the [001] direction of the potential surfaces created by passing a plane through points C, Z_c, and S_a. The energy increment between isolines is 0.2 eV. Isolines for $E=1.2$ eV are highlighted in bold.

space surrounding those points. Figure 5 shows the cross sections of the potential surface by a plane passing through the points Z_c, S_a, and C. This reveals the existence of the two different potential surfaces. One of them corresponds to function $E_z(a,b,c)$, which is defined in the vicinity of Z_c and determines the energy of the z-phase structure, and the second one corresponds to function $E_s(a,b,c)$, which is defined in vicinity of S_a and determines the energy of s-phase structure. The areas of definition of these functions correspond to domains of stability of the two structures with respect to uniform deformations described by variations of the a,b,c parameters.

It is also seen that these domains overlap. However, the two surfaces do not merge together but intersect (two points of intersection are shown in Fig. 5 as P and T). The common points thus found belong to the line of intersection. The existence of such points means that the uniform deformations as themselves do not imply a necessity of the phase transformation. Actually, such deformations can result in the z and s lattices having the same energies and the same unit cells in which the atomic positions stay inherent to the z-phase and the s-phase structures.

Thus it can be concluded that in contrast to a "classic" situation, where the interphase barrier is specified by one potential surface having two potential wells separated in the configuration space and one saddle point associated with transition state, the situation in our study is characterized by presence of two potential wells with overlapping walls. In such a situation, the phase transition should arise when a parent system is impetuously brought by thermal fluctuations to the boundary of stability in the domain of the coexistence of the two phases. Then, after crossing the line of intersection and on approaching the point of instability, the system could spontaneously transform into a lower-energy phase structure. Thus, to reveal this effect theoretically, it is necessary to scan over the boundary of stability of the parent phase in looking for an instability arising at minimal deformation energy. Afterward, the study must be accomplished by the analysis of the atomistic displacement pattern related to such instability in order to check that this would drive the lattice to the daughter structure.

The z-phase and s-phase structures, being deformed via an arbitrary variation of the abc parameters, reduce their starting symmetries from tetragonal D_{4h}^{19} to an orthorhombic D_{2h}^{24} and from tetragonal C_{4h}^{6} to monoclinic C_{2h}^{6}, respectively. It is important that for the s-phase structure, this symmetry reduction gives rise to nonvanishing cross terms between the U_1, U_2, and U_3 deformations related to variation of the abc parameters and one of the shear strains. For the s-phase structure taken within the S_a setting it is the U_4 deformation. This strain was included in the relaxation procedure: for any set of the abc parameters, the s-phase structure was optimized not only with respect to atomic positions but also with respect to α angle between vectors **b** and **c**. The calculations revealed that the α angle variation does not exceed $\pm 4°$ within the whole domain of stability of the s phase, and thus the relevant effects can be neglected. It is important to note that the direct group-subgroup relation occurs between the D_{2h}^{24} and C_{2h}^{6} symmetries, and that the distortion transforming the orthorhombic z lattice into the monoclinic s lattice would belong to the B_{3g} representation of the former lattice.

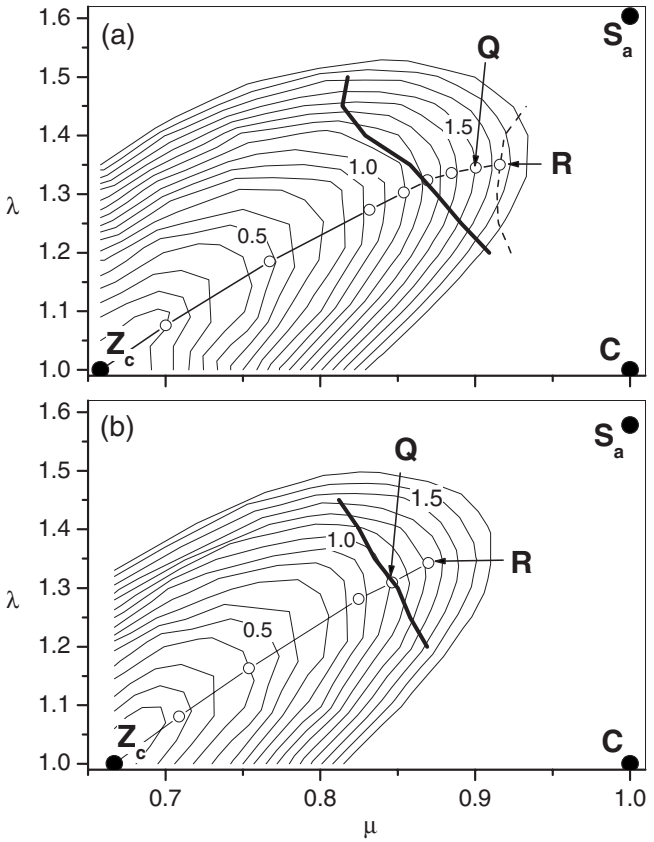

FIG. 6. Potential energy of the z phase $E_z(\lambda,\mu)$ (a) at $P=0$ and (b) at $P=20$ GPa. Bold circles depict points which correspond to the configurations of (c) the z phase (Z_c), s phase (S_a), and cubic phase. The energy increment between isolines is 0.1 eV. The TPB trajectory is plotted with open circles. Bold lines show points at which the relation $E_z(\lambda,\mu)=E_s(\lambda,\mu)$ is fulfilled. The dashed line contains the points at which the soft-mode frequency vanishes.

The complementary information is available if we take into account that the constant pressure condition imposes a constraint on possible variations of the a,b,c parameters. If two new independent variables, $\lambda=a/b$ and $\mu=c/b$, are introduced and if the TPB is considered in the (λ,μ) space, the points C, Z_s, and S_a are specified by coordinates (1,1), (1,0.658), and (1.603,1), respectively. The potential energy of z-phase $E_z(\lambda,\mu)$ calculated at $P=0$ is shown in Fig. 6(a). It is seen that the potential valley of the z phase is markedly elongated toward the S_a point. The line of intersection corresponding to the condition $E_z(\lambda,\mu)=E_s(\lambda,\mu)$ is shown by the bold line.

The area in Fig. 6 covered by isoenergetic lines approximates to the domain of stability of the z-phase structure. According to the model calculations of phonon frequencies and elastic modulus, various types of the lattice destabilization can be found on approaching to any point on the boundary of this area. The instabilities which arise at lowest deformation energy are situated near the point where the boundary crosses the Z_c-S_a line [see the dashed lines in Fig. 6(a)]. They correspond to the soft-mode behavior of the lattice vibration related to the in-phase librations of the SiO_4 tetrahedrons. It is significant that such structural distortion is ex-

actly what is anticipated for the transformation of the Z_c structure into the S_a structure. The point R in Fig. 6(a) corresponds to the point of instability of the z-phase structure with minimal deformation energy. Thus, a trajectory which comes from Z_c point and arrives in R point could be considered as TPB with minimal energy barrier.

The stress tensor calculated for the R-point structure is $(0,-2.6,2.6,0,0,0)$ GPa. This suggests that such a structure may results from the initial z-phase structure in response to external anisotropic stress,

$$\mathbf{S}_2 = (0,-S,S,0,0,0). \tag{9}$$

The calculations (see open circles in Fig. 6) show that the structural evolution, corresponding to external stresses (9) with gradually increasing S values, results in configuration trajectory which passes near the bottom of the potential valley and arrives to the point R Therefore, a detailed analysis of the structural and lattice-dynamical property variations along this trace can provide insight into the microscopic mechanism of the Z_c-S_a transformation.

Theoretically, a structure corresponding to external stresses defined by Eq. (9) would provide a minimum of the $E_z(\lambda,\mu)$ function with respect to λ at fixed μ. So, variable μ can be considered as a coordinate of transformation. The calculated $E_z(\mu)$ dependency is shown in Fig. 7(a) by squares. This trajectory crosses the line of intersection of the two potential surfaces at $\mu=0.87$. This means that for greater μ values, energies of the s-phase structures with the same abc parameters [see triangles in Fig. 7(a)] are lower. Hence, these structures are thermodynamically more preferable.

The crucial factor triggering the process of the $z-s$ transformation was clarified by the results presented in Fig. 7(b). These show [see open circles in Fig. 7(b)] that increasing μ would cause one of the Raman-active vibrational mode, namely, that corresponding to the SiO_4 tetrahedron rotations around the axes parallel to (100), to soften and eventually to vanish at $\mu=0.92$. In the initial z-phase structure this mode belongs to the E_g representation of D_{4h}^{19} symmetry group. In the strained D_{2h}^{24} structure it belongs to the B_{3g} representation. Theoretically, such a mode must be coupled with the U_4 strain, and its softening would drive the lattice unstable against this strain.[25] In line with this, our calculations show that the C_{44} elastic module vanishes at Q point corresponding to $\mu=0.90$ [see black circles as given against the left-hand axis in Fig. 7(b)]. This means that the Q point should be considered as the critical point at which the z structure ceases to be stable against the U_4 shear deformation distorting the orthorhombic unit cell into a monoclinic one, which would be accompanied by the atomic rearrangement process whose onset is mainly related to the eigenvector of the B_{3g} soft mode.[25] The atomic displacement pattern corresponding to this process can be termed as an internal $z-s$ transformations, whereas the preceding uniform deformation of z-phase lattice from the initial stress-free configuration up to point of the lattice destabilization—as an external $z-s$ transformation.

According to our calculations, the deformation energy at Q point is 1.497 eV/molecule. This value can be considered as activation energy for the $z-s$ transformation at $P=0$. Fulfillment of the condition $E_z(\mu)=E_s(\mu)$, which takes place at $\mu=0.87$, corresponds to a deformation energy of 1.202 eV/molecule. This value can be interpreted as energy of the external $z-s$ transformation. The difference $E_z(0.90)-E_z(0.87)=0.295$ eV/molecule can be related to the energy required for initiation of the internal $z-s$ transformation.

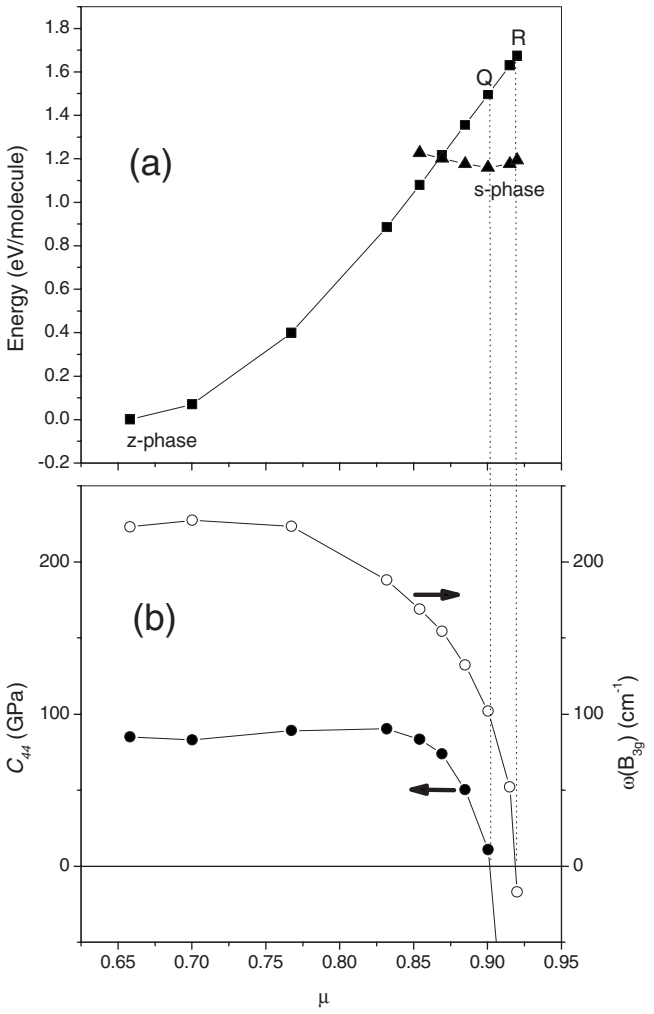

FIG. 7. (a) Variation of energy, soft-mode frequency, and (b) the C_{44} elastic modulus of the z-phase along the TPB. Energies of s-phase structures with the same unit-cell parameters are shown in (a) by triangles.

According to experimental data, the $z-s$ transformation occurs at room temperature only upon hydrostatic compression up to about 20 GPa. This may mean that hydrostatic compression is capable of lowering the $z-s$ energy barrier enough that it can be overcome even at such a low temperature.[7] The effect of pressure on stability of the z phase with respect to finite-scale strains was considered within our model treatment. Figure 6(b) shows the $E_z(\lambda,\mu)$ function calculated at $P=20$ GPa. When comparing Figs. 6(a) and 6(b) one can see that the points Z_c and S_a approach each other with increasing pressure, and simultaneously both the stability domain and the potential-well depth diminish for z phase. The TPB trajectory at $P=20$ GPa stays rather similar to that at $P=0$. According to our calculations, the above discussed instability ($C_{44}\searrow 0$) at $P=20$ GPa arises at a de-

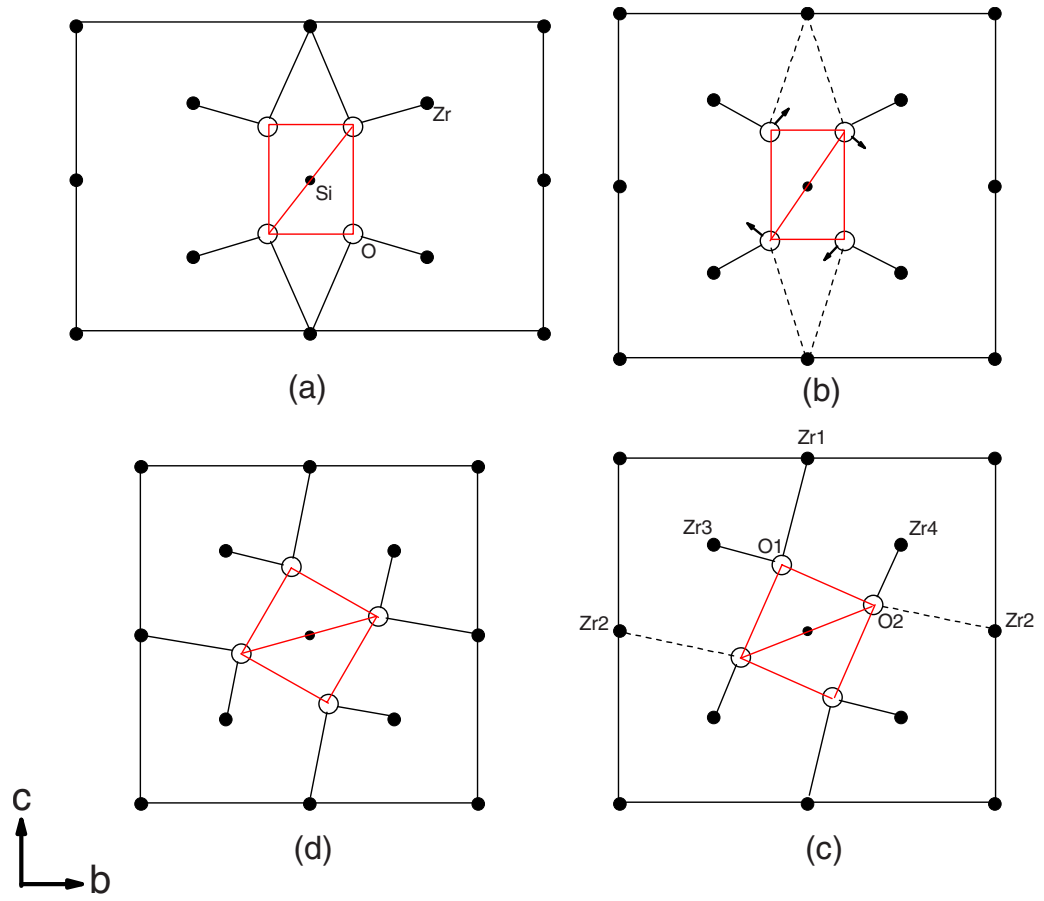

FIG. 8. (Color online) View along the TPB of c cells of various structures: (a) stress-free z phase, (b) z phase at a critical point before internal transformation, (c) s phase at a critical point after internal transformation, and (d) stress-free s phase. Only one of the SiO_4 tetrahedrons is shown. Zr-O bonds shorter and longer than 2.5 Å are shown by solid and dashed lines, respectively. Eigenvector of the soft mode is shown by arrows in (b).

formation energy of 1.021 eV/molecule, which is about 30% lower than at $P=0$. Although it is still higher than thermal energy at room temperature, the tendency toward lowering the activation energy with increasing pressure is well demonstrated. It is worth emphasizing that at $P=20$ GPa the conditions $C_{44}=0$ and $E_z(\mu)=E_s(\mu)$ are fulfilled at about the same μ values. Thus, it can be concluded that at $P=20$ GPa the onset of the internal transformation does not require any additional energy input. It occurs immediately after completion of the external transformation.

As for the s-phase structure, the model calculations allowed us to conclude that the minimal energy instability in s-phase structure (taken in S_a configuration) is induced by the shear stress which obeys the Eq. (9) with $S<0$. Upon decreasing S value the s-phase structure evolves along configuration trajectory which passes in vicinity of the S_a-Z_c line. The elastic instability arises at deformation energy equal to 0.81 eV/molecule. This value must correlate with the activation energy for the $s-z$ transformation. As it was mentioned above, the s phase, which may exists at zero pressure as a metastable phase, returns into the z phase after being heated up to $T=1500$ K.[7] This temperature corresponds to thermal energy of 0.77 eV/molecule. This denotes a good accord between theory and experiment. As a final point of this analysis it can be inferred that the Z_c-S_a trajectory via the Q point passes the lowest-energy barrier separating the z and s structures. This unequivocally means that the relevant TPB should be considered as the most probable TP for the $z-s$ transformation.

C. Atomistic pattern of transformation

Different stages of the atomic arrangement evolution along TPB are represented in Figs. 8(a)–8(d). Fragments of the unit cells of the Z_c and S_a structures in their initial stress-free configurations are shown in Figs. 8(a) and 8(d), respectively. The same structures at a critical point Q just before and after the $z-s$ internal transformation are shown in Figs. 8(b) and 8(c). For transparence, only one of the SiO_4 tetrahedrons with surrounding Zr atoms is shown, thus allowing us to see how the coordination spheres around oxygen atoms change along the TPB [the notation of the atoms is given in Fig. 8(c)].

The first stage of $z-s$ transformation, which has been termed above as external deformation, is represented in Figs. 8(a) and 8(b). It can be seen that the Z_c lattice at the critical point is extended along the c axis and contracted along the b axis as compared with its initial configuration. Such a variation of the cell's shape results in a distortion of the SiO_4 tetrahedrons accompanied by a marked shortening of the

O1-O2 edges, which, indeed, must destabilize the structure. One more source of the destabilization can be revealed in a lengthening of the Zr1-O1 and Zr1-O2 bonds [dashed lines in Fig. 8(b)] so that these Zr···O separation exceeds the lengths typical for Zr-O chemical bonding. These two factors cause the B_{3g} mode mentioned in Sec. III B to soften, thus inducing the $z-s$ transition. The eigenvector of this mode is shown in Fig. 8(b) by arrows, and its detailed analysis can give us a key to understanding the microscopic mechanism of the transition.

First, we note that the lattice being deformed along this eigenvector loses the symmetry operations necessary to keep the O1 and O2 atoms equivalent. Furthermore, this shortens the Zr1···O1 contact, thus retaining a length typical for a Zr-O valence bonding and putting the O1 atom in the position which is characterized, as in initial stress-free state, by the existence of the three valence bonds: Zr1-O1, Zr3-O1, and Si-O1. At the same time, exceptionally intriguing situation arises with atom O2. Actually, the Zr1-O2 bonds break, and the O2 atoms, being connected by only two valence bonds (Zr4-O2 and Si-O2), may freely move to elongate the O1-O2 contact. In doing so, the O2 atom approaches the Zr2 position thus resulting in formation of a new Zr2-O2 valence bond. In fact, this is a crucial moment of the $z-s$ conversion.

The optimized atomic positions arising in course of this process which we have called internal $z-s$ transformation are shown in Fig. 8(c). It is clearly seen that the new atomic arrangement thus formed is very close to that of the S_a structure [shown in Fig. 8(d)]. Figures 8(c) and 8(d) show the final stage of transformation which can be specified as an external s-phase relaxation. Similarly, the inverse $s-z$ transformation may be illustrated by a consequence of Figs. 8(d)–8(a).

The detailed quantitative analysis shows that the rupture of a quarter of the Zr-O bonds accompanied by the formation of the others, which we call as bond-switching process, is a central point of the transformation from the energetic point of view. The anatomy of this process may be illustrated by analysis of the Zr-O bond-length variation along the TPB trajectory. Figure 9 shows the μ dependencies of Zr-O bond lengths. One can see that in the initial z-phase configuration every Zr atom forms eight Zr-O bonds: four relatively shorter ones, Zr3-O1 and Zr4-O2, and four relatively longer ones, Zr1-O1 and Zr1-O2. The elastic strain, which is considered as driving force of the transformation, forces the longer Zr-O bonds to lengthen more thus making the lattice unstable against the U_4 strain. This instability triggers a spontaneous internal transformation which makes the Zr1-O1 and Zr1-O2 bonds nonequivalent: the first ones shorten down to 2.27 Å and the second ones elongate up to 3.17 Å are broken.

An opposite variation is manifested by the Zr2-O1 and Zr2-O2 distances: being rather long (4.06 Å) in the initial z-phase structure, their shorten to 3.43 Å at the critical point. The spontaneous internal transformation forces the Zr2-O1 contacts to lengthen and the Zr2-O contacts to shorten markedly, thus providing a "germ" to formation of new Zr-O valence bonds, which "substitute" the broken ones. A joint consideration of Figs. 8 and 9 allows us to conclude that the central act of the internal $z-s$ transformation consists

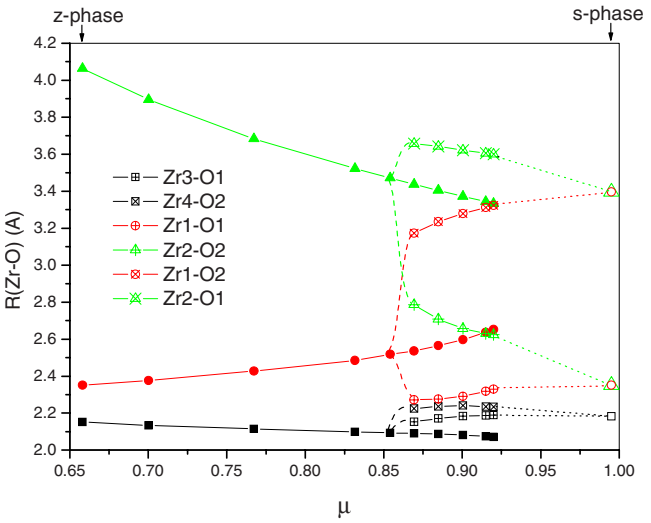

FIG. 9. (Color online) Variations of Zr-O bond lengths along the TPB. Changes which occur during internal transformation are depicted as dashed lines. Changes which take place during s-phase relaxation are shown by dotted lines. For atomic labels, see Fig. 8.

in a concerted displacements of O2 atoms from Zr1 atoms to Zr2 atoms, accompanied by breaking the Zr1-O2 bond and by the formation of the Zr2-O2 bond.

On considering Fig. 8(b), it can be understood that TPA transformation scenario, which retains orientation of the C_4 axis and equivalence of O1 and O2 atoms, implies substitution of the Zr1-O1 and Zr1-O2 bonds by the Zr2-O1 and Zr2-O2 bonds. Thus, it can be concluded that the TPB suggests two elementary bond-switching acts per every Zr atom (or per every SiO_4 tetrahedrons), whereas the TPA transformation necessitates four elementary bond-switching acts per every Zr atom and therefore is energetically more expensive. This seems to be in line with the fact that the latter transformation is found to be energetically twice as expensive as the former [cf. Figs. 3(a) and 7(a)].

IV. SUMMARY AND CONCLUSIONS

In accordance with experiment, the DFT and SM simulations of the two crystalline polymorphs of $ZrSiO_4$, zircon and reidite, have shown that at $P=0$ the potential energy of zircon is lower than that of reidite, whereas the specific volume is 10% greater. The energy difference was estimated at 1.3 and 0.36 eV/molecule by DFT and SM calculations, respectively.

The results of the calculations performed for increasing hydrostatic compression were also in line with experimental evidence. Indeed, they showed that above a pressure estimated at 15 and 10 GPa (by DFT and SM, respectively), the reidite structure is thermodynamically preferred since its enthalpy becomes lower than that of zircon. However, no lattice-dynamical factors which could trigger the $z-s$ transformation were revealed in this manner. Indeed, even at pressure reaching 70 GPa, neither of the polymorphs was found to be mechanically unstable to undergo this structural conversion. This result allowed us to conclude that it is not

necessarily hydrostatic compression which directly inspires the $z-s$ phase transformation. Rather, it was suggested that this phenomenon could be induced by anisotropic strains, which push the system to the limits of mechanical stability. These strains may result from nonhomogeneity of stress distribution arising in real crystals in high-pressure experiments which deal with synthetic powderlike samples[17] or with impure natural samples.[7] These anisotropic strains could bring the system toward the border of mechanic stability. It is logical to expect that these strains would correspond to transformation path of the lowest-energy barrier and thus of the lowest activation energy. So, it is not surprising that they were found to be shear strains. According to our results, such a strain in zircon corresponds to the lattice extension along the $[110]$ or $[1\bar{1}0]$ directions with simultaneous contraction along the $[001]$ direction. In reidite, this strain corresponds to the U_6 shear deformation.

Our calculations show that at the critical values of these strains, one of the eigenvalues of the elastic constant matrix vanishes, and the lattice undergoes spontaneous homogeneous deformation accompanied by internal structural reorganization. During this process, half of the oxygen atoms displace by about 1 Å from their initial positions. Consequently, quarter of Zr-O bonds are broken, and new bonds are formed such that the atomic arrangement characteristic of one phase is transformed into the atomic arrangement characteristic of the other. This bond-switching process results in drastic alternations inside the ZrO_8 polyhedrons, which is a central point of the $z-s$ and $s-z$ transformations.

Since a major part of our calculations were based on the empirical shell-model treatment, we wish to underline here some points which argue for the logical transparency and objectiveness of our results. Actually, the correlation between the sets of the units cell parameters of two lattices offers, in a model-independent manner, only two possibilities to interconnect the corresponding points in configuration space. Refusing a possibility of the phase transition through amorphization, it must be objectively established that this is associated with the anisotropic macroscopic deformations considered in this study. If so, the structural evolution between initial and final structures may pass either in a direct $D_{4h}^{19}-C_{4h}^{6}$ way or via an intermediate crystalline structures having symmetries which are either higher or lower than those of both end structures.

Taking into account that both end structures have center of inversion, it can be assumed that this symmetry invariance is retained in the course of such an evolution. Therefore, by using the table of correlation between the symmetries of the 32 crystallographic classes, one can readily find only one pathway for the $z-s$ transition via an intermediate structure of higher symmetry, namely, $D_{4h}-O_h-C_{4h}$. In a similar manner, only one pathway can be found for the transition via the lower symmetry structures, namely, $D_{4h}-D_{2h}-C_{2h}-C_{4h}$. The two transformation pathways considered in the present paper correspond to these two scenarios of the symmetry evolution.

Finally we wish to point out that the comparison of the z-phase and s-phase structures presented in their standard crystallographic orientations should necessarily confuse a reader since, according to the most probable scenario of the transformation, the tetragonal fourfold c axis of the scheelite-like lattice derives from one of the twofold axes lying in the ab plane of the zircon lattice. Thus, comparison of the unit cells in Fig. 1 should, indeed, have misleading consequences, which was intuitively predicted more than 20 years ago by Kusaba *et al.*[13]

ACKNOWLEDGMENTS

This study was initiated while one of the authors (M.B.S.) was invited as professor of Ecole Nationale Superieure de Ceramique Industrielle (France). He would like to thank the staff of the institute for hospitality and encouragement. We would like also to thank C. Filloux (Princeton University) for careful reading and constructive remarks concerning the text of this paper.

[1] P. Toledano and V. Dmitriev, *Reconstructive Phase Transitions* (World Scientific, Singapore, 1996).
[2] H. T. Stokes, D. M. Hatch, J. Dong, and J. P. Lewis, Phys. Rev. B **69**, 174111 (2004).
[3] A. M. Saitta and F. Decremps, Phys. Rev. B **70**, 035214 (2004).
[4] N. Choudhury and S. L. Chaplot, Phys. Rev. B **73**, 094304 (2006).
[5] X. Wang, I. Loa, K. Syassen, M. Hanfland, and B. Ferrand, Phys. Rev. B **70**, 064109 (2004).
[6] Y. W. Long, L. X. Yang, S. J. You, Y. Yu, R. C. Yu, C. Q. Jin, and J. Liu, J. Phys.: Condens. Matter **18**, 2421 (2006).
[7] E. Knittle and Q. Williams, Am. Mineral. **78**, 245 (1993).
[8] V. Ozolins and A. Zunger, Phys. Rev. Lett. **82**, 767 (1999).
[9] M. Catti, Phys. Rev. Lett. **87**, 035504 (2001).
[10] A. F. Reid and A. E. Ringwood, Earth Planet. Sci. Lett. **6**, 205 (1969).
[11] H. Ozkan and J. C. Jameson, Phys. Chem. Miner. **2**, 215 (1978); M. Catti, Phys. Rev. B **74**, 174105 (2006).
[12] K. Kusaba, Y. Syono, M. Kikuchi, and K. Fukuoka, Earth Planet. Sci. Lett. **72**, 433 (1985).
[13] K. Kusaba, T. Yagi, M. Kikuchi, and Y. Syono, J. Phys. Chem. Solids **47**, 675 (1986).
[14] H. Leroux, W. U. Reimold, C. Koeberl, I. Hornmann, and J.-C. Doukhanl, Earth Planet. Sci. Lett. **169**, 291 (1999).
[15] H. P. Scott, Q. Williams, and E. Knittle, Phys. Rev. Lett. **88**, 015506 (2001).
[16] S. Ono, K. Funakoshi, Y. Nakajima, Y. Tange, and T. Katsura, Contrib. Mineral. Petrol. **147**, 505 (2004).
[17] W. van Westrenen, M. R. Frank, J. M. Hanchar, Y. Fei, R. J. Finch, and C.-S. Zha, Am. Mineral. **89**, 197 (2004).
[18] M. Marqués, M. Flórez, J. M. Recio, L. Gerward, and J. S. Olsen, Phys. Rev. B **74**, 014104 (2006).
[19] J.-P. Crocombette and D. Ghaleb, J. Nucl. Mater. **257**, 282 (1998).

[20] S. L. Chaplot, L. Pintschovius, N. Choudhury, and R. Mittal, Phys. Rev. B **73**, 094308 (2006).
[21] R. Mittal, S. L. Chaplot, R. Parthasarathy, M. J. Bull, and M. J. Harris, Phys. Rev. B **62**, 12089 (2000).
[22] M. D. Segall, P. L. D. Lindan, M. J. Probert, C. J. Pickard, P. J. Hasnip, S. J. Clark, and M. C. Payne, J. Phys.: Condens. Matter **14**, 2717 (2002).
[23] B. Hammer, L. B. Hansen, and J. K. Norskov, Phys. Rev. B **59**, 7413 (1999).
[24] D. R. Hamann, M. Schlüter, and C. Chiang, Phys. Rev. Lett. **43**, 1494 (1979).
[25] A. Mirgorodsky and M. Smirnov, Ferroelectrics **159**, 139 (1994).